ACS Photonics

Letter

pubs.acs.org/journal/apchd5

Inverted-Rib Chalcogenide Waveguides by Solution Process

Yunlai Zha,[†,‡] Pao Tai Lin,[†,§] Lionel Kimerling,[§] Anu Agarwal,[§] and Craig B. Arnold*[,‡]

[‡]Princeton Institute for the Science and Technology of Materials (PRISM), Princeton University, New Jersey 08544, United States

[§]Materials Processing Center, Massachusetts Institute of Technology, Cambridge, Massachusetts 02139, United States

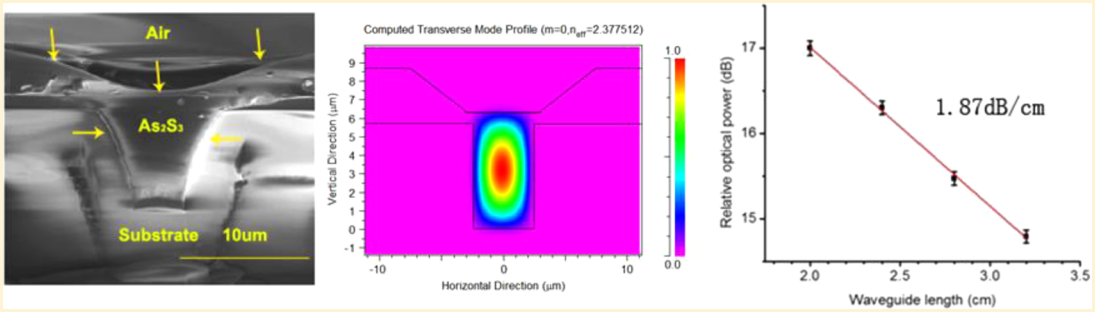

ABSTRACT: This paper studies the fabrication and characterization of solution-processed chalcogenide waveguides by a microtrench filling method. In this process, channels are etched on substrates and backfilled with solution-dissolved arsenic sulfide before being annealed. The waveguides are homogeneous in elemental composition and have good mode confinement. Both simulation and experimental measurements confirm a dominant fundamental mode covering 2.5−2.8 μm. We measure an optical loss of 1.87 dB/cm, which to our knowledge is the lowest among solution-processed waveguides.

KEYWORDS: *chalcogenides, solution-process, glass, microtrench filling, arsenic sulfide*

Chalcogenide glasses are well-known for their excellent transmission in the infrared wavelength regime up to 12 μm, high refractive index, and high optical nonlinearity.[1−4] Such properties have enabled their applications in IR detection, IR fiber transmission, and data storage and sensing, serving a wide variety of industries including health, environment, and security.[5−8] Recently, rapid development expanding on these applications has been fueled by advances in IR laser sources and detectors. To facilitate adoption in this emerging application space, the chalcogenide fabrication process has to offer high performance, reliability, and hybrid integration-compatibility.[9]

None of the current methods for chalcogenide glass deposition command both reliability and hybrid integration-compatibility, for example, with QCLs. For example, traditional methods of vacuum deposition (thermal evaporation, chemical vapor deposition, or sputtering) or pulse laser deposition[10−15] require a substantial investment and elaborate coupling schemes for hybrid component integration. As an alternative with more flexibility, the solution method has been studied extensively for chalcogenide processing.[16−25] With this method, our group demonstrated waveguide integration with quantum cascade lasers (QCL)[26] and another group used arsenic selenide to pattern waveguides.[27] However, in both cases, losses for the solution method are large (4−9 dB/cm) and therefore require improvement in fabrication.

In this paper, we demonstrate a new fabrication scheme for making reliable and low-loss arsenic sulfide waveguides based on a microtrench filling method. Channels are etched in substrates and filled with solution-processed arsenic sulfide before being annealed at an elevated temperature. Both as-deposited films and fabricated waveguides are characterized by optical methods. The simulated mode profile is compared to the profile measured with an IR camera. Waveguide losses are measured and discussed with reference to published results. Our approach significantly reduces the optical loss associated with other solution-processing methods of waveguide fabrication and can be used as a future platform for many on-chip IR devices.

To accurately characterize our samples, we have thoroughly studied the material and optical properties of both as-deposited films and fabricated waveguides. Since residual solvent is a prevalent problem in most solution processed structures, we use 6 h of annealing at 180 °C to ensure optimal removal of solvent.[28] Fourier transform infrared spectroscopy (FTIR) shows that the spin-coated films have a transmission above 80% from 2.5 to 5 μm and over 98% from 2.5 to 2.8 μm, which is our wavelength regime of interest (Figure 1). Our transmission loss values are consistent with or better than other published data.[27−29] The solvent band that is still visible between 2.9 and 3.6 μm as a dip in transmission is mainly due to the aliphatic C−H stretch, but is kept to a minimum. The rest of the band shows excellent transmission and can be safely utilized for device applications. In another test, we dip the processed film into 3% acid solutions for at least 3 min and the films come out intact. This result indicates that, although there still exists trace solvent in the film, its amount is not significant to cause reactions.

Received: November 6, 2013
Published: February 13, 2014

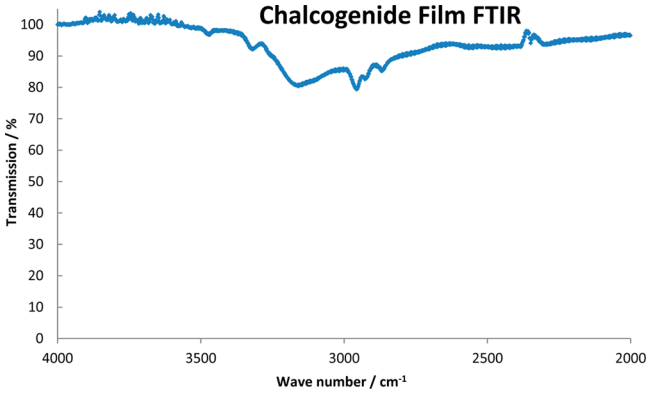

Figure 1. FTIR of 2 μm thick spin-coated films showing high transmission across the spectrum.

Inverted-rib waveguides are fabricated by spin-coating and annealing solution-dissolved chalcogenide in pre-etched channels, as described in Methods. Energy-dispersive X-ray spectroscopy (EDX) mapping is used to verify the material composition. Looking at the cross sections in Figure 2, oxygen

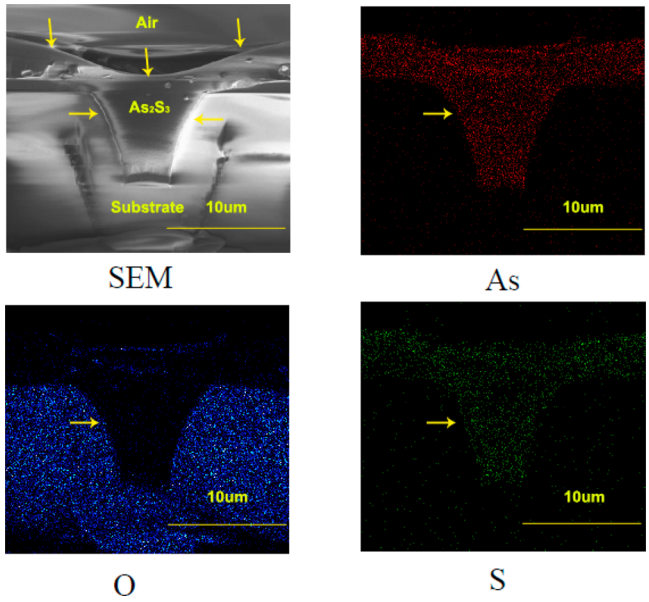

Figure 2. SEM of a waveguide cross-section showing a concave top with the main waveguide region underneath. EDX mapping showing mid-IR lightwave homogeneity of the waveguide.

is found in the substrate structure, whereas the waveguide region only contains arsenic and sulfur. The results show uniform material distribution throughout the waveguide structure and no solvent-specific composition is detected, reaffirming the material integrity of our samples.

In order to characterize the optical properties of our waveguides, we couple a tunable laser from 2.4 to 2.8 μm to the structure. Within the entire wavelength range, a sharp fundamental mode can be clearly resolved. A typical intensity profile of the mode image at λ = 2.6 μm is shown in Figure 3. No major scattering or distortion is observed, which implies that the mid-IR light is well confined inside the waveguides. Furthermore, the fundamental mode remains the dominant one within the wide spectral range, indicating that the waveguides can efficiently transmit mid-IR light.

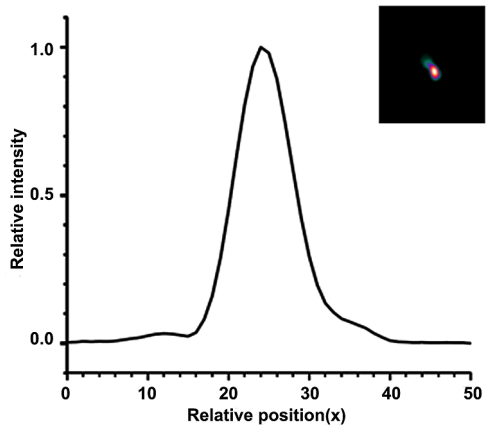

Figure 3. Typical mode output profile measured from infrared images and an infrared camera capture at 2.6 μm. Both show sharp contrast to the background.

Furthermore, we measure the attenuation in optical power through waveguides of differing lengths to determine transmission loss. For this, paper clip structures are used such that a single cleave yields a common facet used for every waveguide, minimizing variations in coupling loss. By fitting the length-dependent optical powers from the waveguide outputs (Figure 4, right), an optical loss as low as 1.87 dB/cm is obtained at λ = 2.6 μm and the same order loss result is found from 2.4 to 2.8 μm. The error bar for the loss measurement is 5%. Solution-processed arsenic selenide waveguides with a similar configuration had a loss of 9 dB/cm at 1.55 μm.[27] Our previous solution-processed waveguides showed 4.52 dB/cm loss on $LiNbO_3$ substrate at 4.8 μm.[26] Such a loss improvement can significantly enhance the usability of these waveguides.

Part of the loss improvement can be attributed to better processing and design. Previously, the waveguides were only heated up to 100 °C and would have a refractive index of 2.15, close to that of the substrate used (lithium niobate). This time, our samples are annealed at 180 °C and have a refractive index of 2.4, much closer to the bulk. Such processing reduces residual solvent and enhances transmission. Moreover, the slab mode is suppressed with our design and material absorption is reduced. Since our waveguide structure is engineered upside-down, the slab part is exposed during annealing. Solvent evaporates during the annealing step causing volume contraction, which results in shrinkage at the main waveguide. This leads to the slab directly above the waveguide bending downward in a concave fashion, as shown in Figure 2. The effect of such a structural difference is modeled in BeamPROP simulation software to predict mode output, using the optical properties (n = 2.4, k = 8 × 10^{-8}) of the materials and approximate shapes of the waveguides.[28,30] The calculated field profiles are displayed in Figure 5, demonstrating the fundamental modes expected from waveguides of such dimensions. A wavelength range from 2.4 to 3.7 μm corresponding to the laser source is simulated for the left structure and shows similar mode profiles, in agreement with our experimental observations. The approximate mode area (intensity above 0.1 from the diagram) is 28 μm^2 for the left structure and 47 μm^2 for the right structure. The direct benefit from the mode area contraction is reduced total material absorption integrated over the entire waveguide. However, it is noted that such structure supports high-order modes. A pure single mode structure would require further dimension

dx.doi.org/10.1021/ph400107s | ACS Photonics 2014, 1, 153−157

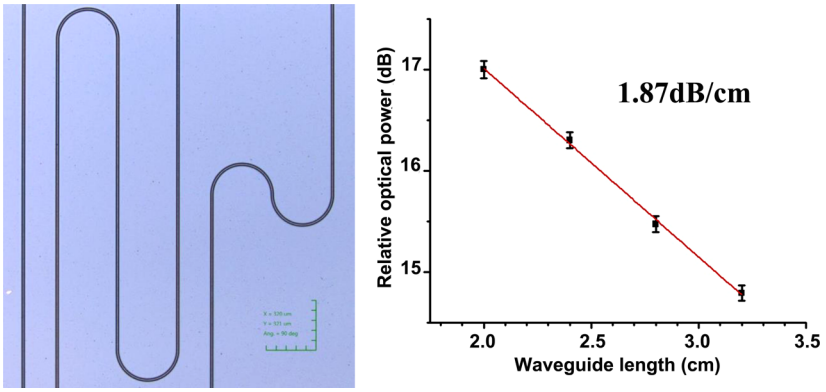

Figure 4. "Paper-clip" waveguide configuration and loss measurement from such waveguides. Left: waveguides of different "paper-clip" sizes have different path lengths; Right: 1.87 dB/cm loss extrapolated from the power attenuation data.

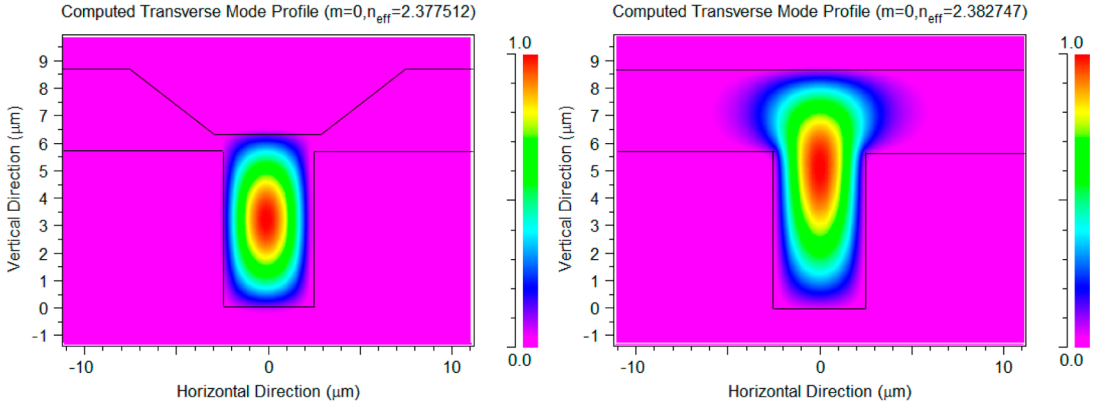

Figure 5. Better mode confinement in our concave-top structure from simulated fundamental mode profiles at $\lambda = 2.6$ μm. Rectangular cross-section is assumed for the waveguides. Left: inverted-rib with a concave top; Right: inverted-rib with a flat top.

reduction. We also notice that it is possible to remove the slab mechanically or chemically by polishing or etching, leaving just the waveguide in the trench. Such a process adds complexity to the overall fabrication process, but not significant improvement in the confinement. Our models show that this ideal waveguide, without a slab, has a mode area of about 26 μm^2, which is very close to our existing structure.

Overall, we can obtain mid-IR solution-processed chalcogenide waveguides reproducibly, without apparent size limitation. This work has demonstrated a low-cost, reliable, and highly efficient method to achieve mid-infrared on-chip photonic structures, offering hybrid integration compatibility and flexibility with lower loss compared to other solution-processed waveguides.

METHODS

Metal basis arsenic sulfide pieces (As_2S_3, Alfa Aesar) are dissolved with propylamine solution at a concentration of 2 g/10 mL. The dissolution takes a few days in a sealed glass bottle, and a magnetic stirrer can be used to expedite the process. The stock solution is passed through 0.1 μm filters and ~10% ethylenediamine is added to minimize pore formation.[31] The silicon dioxide layer is prepared by plasma-enhanced chemical vapor deposition (PECVD) and reactive ion etching. The precursor gases used were N_2O and SiH_4 and the deposition rate is 450 nm/min. The channel structures are transferred from photoresist into the SiO_2 layer through an optimized inductively coupled plasma reactive ion etching (ICP-RIE) process in $Ar/H_2/CHF_3/CF_4$ with flow rates of 6/30/50/2 sccm, respectively. The channel cross section has an inverted isosceles trapezoid shape of 8 μm height, 8 μm top, and 5 μm bottom. The prepared solution is then drop-casted onto a substrate and spun at 1500−2500 rpm for 10 s. Alternatively, one could use doctor blade, drop casting, and so on to backfill the trench with solution. The resulting film is soft-baked under vacuum at 60 °C for 1 h to remove most of the solvent, followed by heat treatment at 180 °C for 6 h to further densify the glass. Vacuum pressure is set around 50 Torr. All preparation and fabrication steps are performed in a glovebox connected to a vacuum oven, so that the material is exposed to minimum levels of oxygen and moisture. More importantly, a glovebox environment protects researchers from directly contacting the material. In our study, FTIR spectra are taken with a Nicolet 8700 by subtracting the substrate spectra from the sample spectra. The data is processed by including a correction due to the Fresnel reflections. Given the arsenic sulfide refractive index of 2.4 and the lithium niobate substrate refractive index of 2.15, the normal reflectance from the chalcogenide surface, the chalcogenide-substrate surface, and the substrate-only front surface is calculated to be 17.0, 0.3, and 13.3%, respectively. Hence, the correction is determined by adding the reflectance of the chalcogenide and chalcogenide-substrate surfaces and subtracting the substrate-only surface, yielding a total of 4.0%. Scanning electron microscope (SEM) images are taken with a Quanta 200 FEG environmental SEM at 15 keV in high vacuum mode. The SEM is equipped with an EDX system for compositional analysis. Film thickness is

dx.doi.org/10.1021/ph400107s | ACS Photonics 2014, 1, 153−157

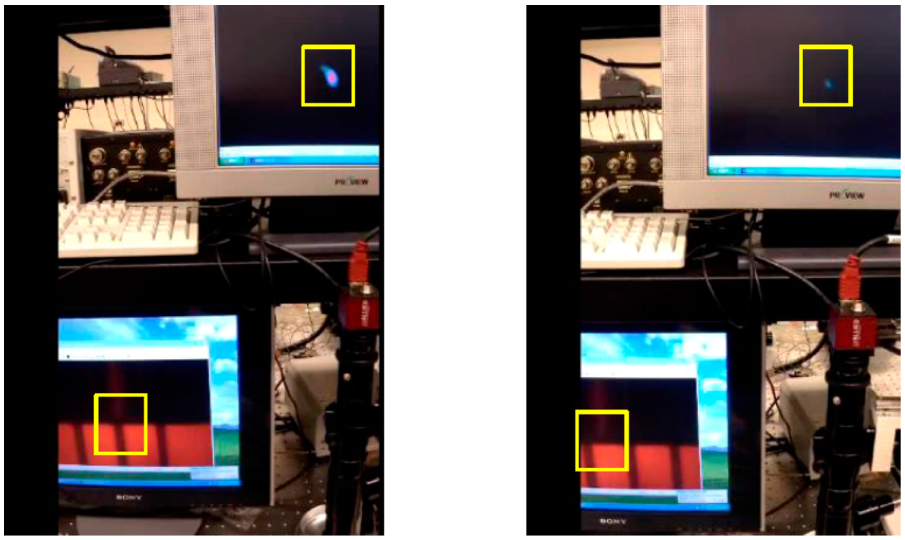

Figure 6. Measurement setup and mode observation at different alignment configurations for efficient coupling. Left: fundamental mode observed when fiber is aligned with the waveguide; Right: mode disappears when misaligned.

measured with an Olympus Laser Confocal Microscope, LEXT OLS4000, by scanning the step height of a scratched film.

The experimental setup for evaluating the waveguide performance involves a mid-IR test platform, as illustrated in Figure 6. The light source is a pulsed laser with 150 mW average power and the laser wavelength is tunable from λ = 2.4 to 3.7 μm. Using a reflective lens, the light is first collimated into a 9 μm core and 125 μm cladding single-polarization fluoride fiber, and then butt coupled into the waveguide. The core of the mid-IR fiber is lined up with the smooth cleaved front facet of the waveguide. Alignment between the optical fiber and the waveguide is achieved using high-precision positioning stages and the fine adjustment is monitored by an upper microscope equipped with a long working distance objective. The mid-IR signals from the waveguides are focused by a calcium fluoride biconvex lens and then imaged by an InSb camera.

AUTHOR INFORMATION

Corresponding Author

*E-mail: cbarnold@princeton.edu. Tel.: (609) 258-1089. Fax: (609) 258-5877.

Author Contributions

†These authors contributed equally to this work (Y.Z. and P.T.L.).

Notes

The authors declare no competing financial interest.

ACKNOWLEDGMENTS

This work is supported by NSF Grant EEC-0540832 through the Mid-Infrared and Technologies for Health and Environment (MIRTHE) center. The authors also acknowledge funding support from the Defense Threat Reduction Agency under Award Nos. HDTRA1-10-1-0101 and HDTRA1-13-1-0001. The authors acknowledge the use of the PRISM Imaging and Analysis Center, which is supported in part by the Princeton Center for Complex Materials, NSF Grant DMR-0819860.

REFERENCES

(1) Petkov, K.; Ewen, P. J. S. Photoinduced changes in the linear and non-linear optical properties of chalcogenide glasses. *J. Non-Cryst. Solids* **1999**, *249*, 150−159.

(2) Owen, A. E.; Firth, A. P.; Ewen, P. J. S. Photoinduced structural and physicochemical changes in amorphous-chalcogenide semiconductors. *Philos. Mag. B* **1985**, *52*, 347−362.

(3) Kohoutek, T.; Orava, J.; Prikryl, J.; Wagner, T.; Frumar, M. All-chalcogenide middle infrared dielectric reflector and filter. *J. Non-Cryst. Solids* **2011**, *357*, 157−160.

(4) Sojka, L.; Tang, Z.; Zhu, H.; Beres-Pawlik, E.; Furniss, D.; Seddon, A. B.; Benson, T. M.; Sujecki, S. Study of mid-infrared laser action in chalcogenide rare earth doped glass with Dy^{3+}, Pr^{3+}, and Tb^{3+}. *Opt. Mater. Express* **2012**, *2*, 1632−1640.

(5) Eggleton, B. J.; Luther-Davies, B.; Richardson, K. Chalcogenide photonics. *Nat. Photonics* **2011**, *5*, 141−148.

(6) Eggleton, B. J. Chalcogenide photonics: fabrication, devices and applications Introduction. *Opt. Express* **2010**, *18*, 26632−26634.

(7) Grillet, C.; Lee, M. W.; Gai, X.; Tomljenovic-Hanic, S.; Monat, C.; Magi, E.; Moss, D. J.; Eggleton, B. J.; Madden, S.; Choi, D. Y.; Bulla, D.; Luther-Davies, B., Chalcogenide glass photonic crystals: progress and prospects. *Proc. SPIE* **2010**, *7609*.

(8) Juejun, H.; Carlie, N.; Petit, L.; Agarwal, A.; Richardson, K.; Kimerling, L. C.; Cavity-Enhanced, I. R. Absorption in planar chalcogenide glass microdisk resonators: experiment and analysis. *J. Lightwave Technol.* **2009**, *27*, 5240−5245.

(9) Zha, Y. L.; Waldmann, M.; Arnold, C. B. A review on solution processing of chalcogenide glasses for optical components. *Opt. Mater. Express* **2013**, *3*, 1259−1272.

(10) Hu, J. J.; Musgraves, J. D.; Carlie, N.; Zdyrko, B.; Luzinov, I.; Agarwal, A.; Richardson, K.; Kimerling, L. Development of chipscale chalcogenide glass based infrared chemical sensors *Proc. SPIE* **2011**, 7945, DOI: 10.1117/12.871399

(11) Balan, V.; Vigreux, C.; Pradel, A. Chalcogenide thin films deposited by radio-frequency sputtering. *J. Optoelectron. Adv. Mater.* **2004**, *6*, 875−882.

(12) Youden, K. E.; Grevatt, T.; Eason, R. W.; Rutt, H. N.; Deol, R. S.; Wylangowski, G. Pulsed-laser deposition of Ga-La-S chalcogenide glass thin-film optical wave-guides. *Appl. Phys. Lett.* **1993**, *63*, 1601−1603.

(13) Hu, J. J.; Tarasov, V.; Agarwal, A.; Kimerling, L.; Carlie, N.; Petit, L.; Richardson, K. Fabrication and testing of planar chalcogenide waveguide integrated microfluidic sensor. *Opt. Express* **2007**, *15*, 2307−2314.

(14) Richardson, K.; Petit, L.; Carlie, N.; Zdyrko, B.; Luzinov, I.; Hu, J.; Agarwal, A.; Kimerling, L.; Anderson, T.; Richardson, M. Progress on the fabrication of on-chip, integrated chalcogenide glass (Chg)-based sensors. *J. Nonlinear Opt. Phys.* **2010**, *19*, 75−99.
(15) Lin, H. T.; Li, L.; Zou, Y.; Danto, S.; Musgraves, J. D.; Richardson, K.; Kozacik, S.; Murakowski, M.; Prather, D.; Lin, P. T.; Singh, V.; Agarwal, A.; Kimerling, L. C.; Hu, J. J. Demonstration of high-Q mid-infrared chalcogenide glass-on-silicon resonators. *Opt. Lett.* **2013**, *38*, 1470−1472.
(16) Markos, C.; Yannopoulos, S. N.; Vlachos, K. Chalcogenide glass layers in silica photonic crystal fibers. *Opt. Express* **2012**, *20*, 14814−14824.
(17) Chern, G. C.; Lauks, I. Spin coated amorphous chalcogenide films: Structural characterization. *J. Appl. Phys.* **1983**, *54*, 2701.
(18) Chern, G. C.; Lauks, I.; McGhie, A. R. Spin coated amorphous chalcogenide films: Thermal properties. *J. Appl. Phys.* **1983**, *54*, 4596.
(19) Zenkin, S. A.; Mamedov, S. B.; Mikhailov, M. D.; Turkina, E. Y.; Yusupov, I. Y. Mechanism for interaction of amine solutions with monolithic glasses and amorphous films in the As-S system. *Glass Phys. Chem.* **1997**, *23*, 393−399.
(20) Orava, J.; Wagner, T.; Krbal, A.; Kohoutek, T.; Vlcek, M.; Frumar, M. Selective wet-etching and characterization of chalcogenide thin films in inorganic alkaline solutions. *J. Non-Cryst. Solids* **2007**, *353*, 1441−1445.
(21) Mamedov, S. On the macromolecular mechanism of dissolution of As_2S_3 films in organic solutions. *Thin Solid Films* **1993**, *226*, 215−218.
(22) Kohoutek, T.; Orava, J.; Sawada, T.; Fudouzi, H. Inverse opal photonic crystal of chalcogenide glass by solution processing. *J. Colloid Interface Sci.* **2011**, *353*, 454−458.
(23) Carlie, N.; Musgraves, J. D.; Zdyrko, B.; Luzinov, I.; Hu, J. J.; Singh, V.; Agarwal, A.; Kimerling, L. C.; Canciamilla, A.; Morichetti, F.; Melloni, A.; Richardson, K. Integrated chalcogenide waveguide resonators for mid-IR sensing: Leveraging material properties to meet fabrication challenges. *Opt. Express* **2010**, *18*, 26728−26743.
(24) Kohoutek, T.; Wagner, T.; Vlcek, M.; Vlcek, M.; Frumar, M. Spin-coated $As_{33}S_{67-x}Se_x$ thin films: The effect of annealing on structure and optical properties. *J. Non-Cryst. Solids* **2006**, *352*, 1563−1566.
(25) Waldmann, M.; Musgraves, J. D.; Richardson, K.; Arnold, C. B. Structural properties of solution processed $Ge_{23}Sb_7S_{70}$ glass materials. *J. Mater. Chem.* **2012**, *22*, 17848−17852.
(26) Tsay, C.; Zha, Y.; Arnold, C. B. Solution-processed chalcogenide glass for integrated single-mode mid-infrared waveguides. *Opt. Express* **2010**, *18*, 26744−26753.
(27) Zou, Y.; Lin, H.; Ogbuu, O.; Li, L.; Danto, S.; Novak, S.; Novak, J.; Musgraves, J. D.; Richardson, K.; Hu, J. Effect of annealing conditions on the physio-chemical properties of spin-coated As_2Se_3 chalcogenide glass films. *Opt. Mater. Express* **2012**, *2*, 1723−1732.
(28) Song, S.; Dua, J.; Arnold, C. B. Influence of annealing conditions on the optical and structural properties of spin-coated As_2S_3 chalcogenide glass thin films. *Opt. Express* **2010**, *18*, 5472−5480.
(29) Zha, Y.; Arnold, C. B. Solution-processing of thick chalcogenide-chalcogenide and metal-chalcogenide structures by spin-coating and multilayer lamination. *Opt. Mater. Express* **2013**, *3*, 309−317.
(30) Tsay, C. R. *Processing soft materials for integrated photonic and macroelectronic components and devices*; Princeton University: New Jersey, 2011.
(31) Zha, Y.; Fingerman, S.; Cantrell, S. J.; Arnold, C. B. Pore formation and removal in solution-processed amorphous arsenic sulfide films. *J. Non-Cryst. Solids* **2013**, *369*, 11−16.